PREPARATION AND STUDY OF Mg$_2$Sn-BASED COMPOSITES WITH DIFFERENT COMPOSITIONS

PRIPRAVA IN KARAKTERIZACIJA LASTNOSTI KOMPOZITOV NA OSNOVI Mg2Sn

Varužan Kevorkijan[1], Srečo Davor Škapin[2]

[1]zasebni raziskovalec, Betnavska cesta 6, 2000 Maribor, Slovenia
[2]Srečo Davor Škapin, Institut "Jožef Stefan", Jamova 39, 1000 Ljubljana, Slovenia
varuzan.kevorkijan@impol.si

Single-phase Mg$_2$Sn powders were successfully reaction-synthesized from the elements and applied for the preparation of Mg$_2$Sn-based composites with different natures, microstructures and combinations of properties. These were fully dense ($\geq$95 % T.D.) Mg- and Al-metal-matrix composites (MMCs) reinforced with either Mg$_2$Sn particles or mixtures of Mg$_2$Sn with TiC or TiB$_2$ particulates by the infiltration of porous Mg$_2$Sn preforms with molten magnesium or aluminium; and (ii) Mg$_2$Sn intermetallic matrix composites discontinuously reinforced with TiC and TiB$_2$ particles by pressureless sintering.
The microstructures of the composite samples were examined using scanning electron microscopy (SEM-EDS) and X-ray powder diffraction (XRD). The mechanical properties were evaluated by Vickers hardness measurements performed at room temperature, while the fracture toughness of the specimens was determined by applying the indentation method.
Based on the data accumulated, an evaluation of the mechanical properties of these composites on the basis of the volume content of different constituents was performed.
Moreover, the ability of various microstructures obtained with pressureless infiltration and sintering for tailoring the desired combination of mechanical properties. (e.g., toughening in combination with hardness) was also investigated and reported.
Thus, the infiltration led to MMCs with different microstructures and mechanical properties, depending on the infiltrant applied. The samples infiltrated with molten magnesium possessed a characteristic lamellar, sometimes referred to as "Chinese script", eutectic microstructure and thereby an enhanced fracture toughness (up to 7.7 MPa m$^{1/2}$ in non-reinforced and 5.8 MPa·m$^{1/2}$ in reinforced counterparts), in combination with a Vickers hardness superior to those of conventional Mg-Sn alloys. On the other hand, although the mechanical response (Vickers hardness) of the samples infiltrated with aluminium was even better than in the counterparts infiltrated with magnesium, the absence of the "Chinese script" microstructure was observed to have a detrimental influence on the fracture toughness, which was significantly lower in these samples.
The densification of intermetallic matrix composites (IMCs) with a Mg$_2$Sn matrix discontinuously reinforced with TiC or TiB$_2$ ceramic reinforcement performed by non-reactive, solid-state sintering resulted in samples with a high density ($\geq$95% T.D.) and different combinations of mechanical properties compared to MMCs obtained by infiltration. The Vickers hardnesses of the sintered IMCs were much better than in the MMCs obtained by infiltration, with the exception of the fracture toughness, which was reduced below 1.8 MPa m$^{1/2}$.

Key words: Mg$_2$Sn powder, synthesis, Mg$_2$Sn-based composites, sintering, infiltration, microstructure development, hardness, fracture toughness

Z reakcijo v trdnem smo iz elementov sintetizirali Mg$_2$Sn. Spojino smo zdrobili in prah uporabili za pripravo vrste kompozitov z različnimi mikrostrukturnimi in mehanskimi lastnostmi. Pripravili smo goste kompozite ($\geq$95 % T. G.): (i) na osnovi kovinske matrice Mg in Al tako, da smo v porozne predoblike spojine Mg$_2$Sn ter predoblike različnih sestav na osnovi Mg$_2$Sn in TiC oziroma TiB$_2$ infiltrirali tekoči Mg oziroma Al, in (ii) na osnovi intermetalne spojine Mg$_2$Sn, ki smo jih pripravili s sintranjem Mg$_2$Sn z dodatkom ojačitvene faze trdin TiC oziroma TiB$_2$.
Mikrostrukturno analizo pripravljenih kompozitov smo opravili z vrstičnim elektronskim mikroskopom in elementno spektroskopsko disperzijsko analizo (EDS) ter z rentgensko praškovno difrakcijo. Mehanske lastnosti, trdoto po Vickersu in zlomno žilavost smo merili pri sobni temperaturi.
Dobljene rezultate smo razložili glede na fazno sestavo pripravljenih kompozitnih vzorcev. Opisali smo odvisnost mehanskih lastnosti infiltriranih in sintranih vzorcev v odvisnosti od mikrostrukturnih karakteristik.
Pri infiltraciji nastajajo kompoziti s kovinsko matrico (KKM) z različno mikrostrukturo in mehanskimi lastnostmi, kar je odvisno od uporabljene kovine, ki jo infiltriramo. Kompoziti na osnovi Mg izkazujejo lamelarno evtektično mikrostrukturo (kitajska pismenka) in izboljšano zlomno žilavost (do 7,7 MPa m$^{1/2}$ neojačani materiali in 5,8 MPa m$^{1/2}$ ojačani kompozitni materiali) in tudi višjo trdnost po Vickersu glede na komercialne Mg-Sn zlitine. Kompoziti na osnovi infiltriranega Al izkazujejo višjo trdnost kot Mg kompoziti, vendar pa nižjo zlomno žilavost, ker ne tvorijo lamelarne mikrostrukture.
Pri sintranju kompozitov na osnovi intermetalne Mg$_2$Sn-matrice, ki so bili ojačani s TiC oziroma TiB$_2$ nastajajo gosto sintrani kompozitni materiali ($\geq$95 % T. G.) z različnimi mehanskimi lastnostmi. Trdota teh materialov je večja, kot jo izkazujejo kompoziti na osnovi kovinske matrice, vendar pa imajo manjšo zlomno žilavost, manj kot 1,8 MPa m$^{1/2}$.

Ključne besede: Mg$_2$Sn-prah, priprava, kompoziti na osnovi Mg$_2$Sn, sintranje, infiltracija, razvoj mikrostrukture, trdota, prelomna žilavost

1 INTRODUCTION

Current applications of magnesium stannide (Mg$_2$Sn) are limited to the optimisation of the microstructure and mechanical properties of magnesium [1–7] and in lead-free aluminium alloys [8]. In the Mg-Sn and Mg-Sn-Ca creep-resistant magnesium alloys, Mg$_2$Sn precipitates are applied as a thermally stable intermetallic phase for suppressing the grain-boundary sliding and dislocation movement, resulting in an improvement of the creep properties.

However, due to its high melting point (770 °C), relatively low density (3.59 g/cm^3 – about half that of the density of tin), excellent compressibility (2.83 10^{-11} m^2/N, approximately 50 % higher than for Mg$_2$Si) and a thermal expansion coefficient (9.9 10^{-6} K^{-1}) similar to some borides and carbides [9,10], magnesium stannide is a promising structural material, particularly in combination with magnesium and aluminium alloys and composites. The Vickers hardness of Mg$_2$Sn is about 1.2 GPa [7], significantly lower than for Mg$_2$Si (3.5–7.0 GPa), but still twice as high in comparison with the hardness of Mg-Sn alloys.

In addition, Mg$_2$Sn is a stoichiometric compound suitable for achieving characteristic eutectic microstructures (i.e., "Chinese-script") and therefore for tailoring the properties of composites (particularly the fracture toughness) with Mg$_2$Sn appearing as a matrix or a reinforcement phase.

In contrast to numerous investigations carried out in developing Mg-Sn alloys with Mg$_2$Sn precipitates formed *in situ*, only a limited number of investigations were concerned with the synthesis of Mg$_2$Sn powder [11] and, to the best of our knowledge, none with its densification, alone or with some other reinforcing phases, i.e., as a matrix for high-temperature composites or as particulate reinforcement in metal matrix composites.

Hence, in the present study, the following investigations were performed in order to demonstrate the potential of Mg$_2$Sn as an advanced composite matrix or discontinuous reinforcement: (i) the synthesis of Mg$_2$Sn single-phase powder from the elements; (ii) pressureless sintering and characterisation of Mg$_2$Sn-based intermetallic matrix composites discontinuously reinforced with TiC or TiB$_2$ particles, and (iii) the formation and characterisation of Mg- or Al-metal matrix composites reinforced with either Mg$_2$Sn particles or mixtures of Mg$_2$Sn with TiC or TiB$_2$ particulates by the infiltration of porous Mg$_2$Sn preforms with molten magnesium and aluminium.

2 EXPERIMENTAL

In the first part of the experimental work, Mg$_2$Sn powder was synthesized with a reaction synthesis from the elements. As the source of magnesium and tin, cylindrical samples machined from pure magnesium and tin rods were used. Magnesium and tin samples in three different molar ratios (stoichiometric, with 5 % and 10 % excess of magnesium) were placed in a platinum crucible and heated in a vacuum furnace (for 2 h at 660 °C or for 1 h at 700 °C) in a static atmosphere of argon. This was followed by cooling to room temperature and characterisation of the as-obtained product with optical and scanning electron microscopy (OM and SEM) and X-ray diffraction (XRD). After that, the product was milled in an attrition mill for various milling times (0.5–2 h) in order to achieve the desired morphology of the Mg$_2$Sn

particles. The as-milled Mg$_2$Sn powders were then applied for various infiltration and sintering experiments.

The infiltration was performed by using porous preforms made from laboratory synthesized Mg$_2$Sn powder of grade C (**Table 1**) and mixtures of Mg$_2$Sn powder grade C and commercially available TiC (99.5 %, d_{50} = 4 μm) and TiB$_2$ powders (99.5 %, d_{50} = 6 μm), as listed in **Table 2**. The preforms were isostatically pressed at various pressures (from 80 MPa to 150 MPa) in order to achieve samples with different porosities. The samples obtained were cylinders, 50 mm high and 20 mm in diameter. As infiltrant, Al-xSn and Mg-xSn (x = 3%, 5 %) alloys were applied. Al-xSn and Mg-xSn alloys necessary for infiltration were prepared from pure aluminium or magnesium and pure tin powders melted in a graphite crucible with the protection of a fusing agent. The melt was then stirred to ensure homogeneity and, finally, it was cast into a preheated mould. The as-cast ingots were cut and machined into thin cylindrical plates having the same diameter as the Mg$_2$Sn preforms (20 mm). Finally, a preform sandwiched between two Al-xSn or Mg-xSn plates was placed in a ceramic crucible using the following procedure: the first Al-xSn or Mg-xSn plate was placed on the bottom of crucible and the preform was fixed on it using upper and lower preformatted steel plates. After that, the upper Al-xSn or Mg-xSn plate was placed on it. The volume of the Al-xSn or Mg-xSn plates was calculated to be approximately 50 % higher than the volume of the pores in the preform. The infiltration was conducted by heating the assembly in a vacuum furnace at 730 °C for 1 h, under a static atmosphere of argon.

After completion of the infiltration, the assembly was cooled to room temperature, and then the infiltrated preform was removed from the furnace. The green samples for sintering experiments were formulated by blending the synthesized Mg$_2$Sn powder (grade C, **Table 1**) with commercial ceramic powders (TiC and TiB$_2$) in appropriate amounts to create IMCs with mass fractions w = (10, 30 and 50) % of TiC or TiB$_2$ reinforcement. The powder blends were thoroughly mixed in a planetary mill and subsequently cold compacted. In all cases, the sintering of the compacts was conducted at 750 °C for 1 h in a static atmosphere of argon using a vacuum furnace. The as-synthesized composite samples were cut, machined and polished in accordance with standard procedures.

Microstructural characterization of the fabricated composites was performed with OM and SEM, whereas XRD measurements were applied to the samples to identify the phases and their crystal structure. A quantitative determination of the volume percentage of Mg$_2$Sn and ceramic particles in the matrix, as well as the retained porosity, was performed with an assessment of optical and scanning electron micrographs of polished composite bars using the point-counting method and image analysis and processing software. The composite

density measurements were carried out using Archimedes' principle, applying absolute ethanol as the immersion fluid. The initial density of the green compacts (preforms and tablets) was calculated from the mass and geometry of the samples.

Vickers hardness (HV) measurements were performed at room temperature on polished composite samples and calculated as the average of six indentations. These measurements were made with a conventional Vickers tester (load: 9.8–24.5 N for 15 s).

Due to their small dimensions and high brittleness, the fracture toughness of the specimens obtained was determined by applying the indentation method [12]. The K_{IC} of the composite samples was determined from submicron-derived indentation cracks and calculated according to the equations proposed by Niihara et al. [13].

3 RESULTS AND DISCUSSION

3.1 Mechanism of the formation, chemical composition and morphology of laboratory-prepared Mg₂Sn powder

Depending on the initial composition of the reaction mixture and the heating conditions, the concentration of Mg and Sn impurities in the synthesized Mg₂Sn phase varied significantly.

On applying reaction mixtures with a stoichiometric ratio of elemental magnesium and tin, more than $w = 5$ % of the tin remained in the reaction product obtained (Mg₂Sn powder grade A, **Table 1**), which was most probably caused by a loss of magnesium. This assumption was additionally confirmed by the experimental finding that the amount of non-reacted tin increased with the increasing temperature of the synthesis.

Table 1: Phase composition and morphology of laboratory-prepared Mg₂Sn powders
**Tabela 1:** Fazna sestava in morfologija laboratorijsko izdelanih Mg₂Sn prahov

Powder	$\varphi(Mg_2Sn)$/%	$\varphi(Sn)$/%	d_{50}/μm
Grade A	95	5	3.3
Grade B	97	3	2.4
Grade C	99.8	0.2	2.1

On the other hand, by applying a reaction mixture with a small ($x = 5$ %) excess of magnesium, the amount of non-reacted tin was reduced below 5 % or even below $w = 3$ % (mass fractions) (grade B, **Table 1**) at a lower temperature of synthesis (660 °C).

Finally, by using a reaction mixture with the mol fraction $x = 10$ % excess of magnesium, single-phase Mg₂Sn (grade C, **Table 1**) with no Mg or Sn peak detected in the XRD pattern was prepared at 700 °C.

The investigation of the solidified product samples indicated that the reaction mechanism of the Mg₂Sn synthesis is homogeneous nucleation and growth. Based on the phase diagram of the Sn-rich corner in the Mg-Sn

binary system [14], it is evident that Mg will start to dissolve into the liquid phase immediately after the temperature exceeds the melting point of Sn (505 K). With increasing temperature, a greater amount of Mg will be dissolved and, after melt saturation, the Mg₂Sn will start to nucleate according to reaction 1:

$$Mg_{(s)} + Sn_{(l)} = Mg_2Sn_{(s)} \tag{1}$$
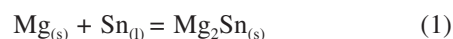
Above the melting point of magnesium (923 K), the nucleation of Mg₂Sn will continue by nucleation from the saturated liquid phase according to reaction 2:

$$Mg_{(l)} + Sn_{(l)} = Mg_2Sn_{(s)} \tag{2}$$

Thus, to achieve the complete conversion of reactants into Mg₂Sn, it is important to preserve a permanent excess of magnesium (approximately $w = 10$ %) in the system up to the end of the synthesis. The morphology of the laboratory-prepared Mg₂Sn powder, obtained with milling the solidified sample from reactive synthesis, is presented in **Figure 1**. As is evident, the powder obtained is non-agglomerated, with well-shaped individual particles with a size below 5 μm.

The typical phase composition in the synthesized Mg₂Sn powders is reported in **Table 1**. The compositions of various Mg₂Sn-TiC and Mg₂Sn-TiB₂ mixtures used for preforms in the infiltration experiments are listed in **Table 2**.

Table 2: The composition of various Mg₂Sn-TiC and Mg₂Sn-TiB₂ mixtures used for preforms preparation in the infiltration experiments
Tabela 2: Sestava različnih zmesi Mg₂Sn-TiC in Mg₂Sn-TiB₂, uporabljenih za pripravo predoblik

Mixture	Initial composition, φ/%
#1	100 % Mg₂Sn (grade C)
#2	75 % Mg₂Sn (Grade C)–25 % TiC
#3	75 % Mg₂Sn (Grade C)– 25 % TiB₂
#4	70 % Mg₂Sn (Grade C)–30 % TiC
#5	70 % Mg₂Sn (Grade C)–30 % TiB₂

3.2 Composites made by pressureless infiltration

3.2.1 Al-Mg₂Sn₍ₚ₎ and Mg-Mg₂Sn₍ₚ₎

The infiltration of porous Mg₂Sn preforms (composition #1, **Table 2**) with molten Al resulted in fully dense composite samples with a continuous aluminium-based matrix, reinforced with Mg₂Sn particles and Mg₂Sn precipitates appearing near the primary Mg₂Sn particles, **Figure 2a**.

On the other hand, samples fully infiltrated with molten magnesium have a characteristic lamellar "Chinese script" eutectic microstructure, **Figure 3a**, and completely different mechanical properties, **Table 3**.

In both cases, due to the complete and non-reactive wetting of the Mg₂Sn preform skeleton with molten Mg or Al, under atmospheric pressure the infiltration proceeded spontaneously. The absence of chemical reactions between the preform skeleton and the molten infiltrants
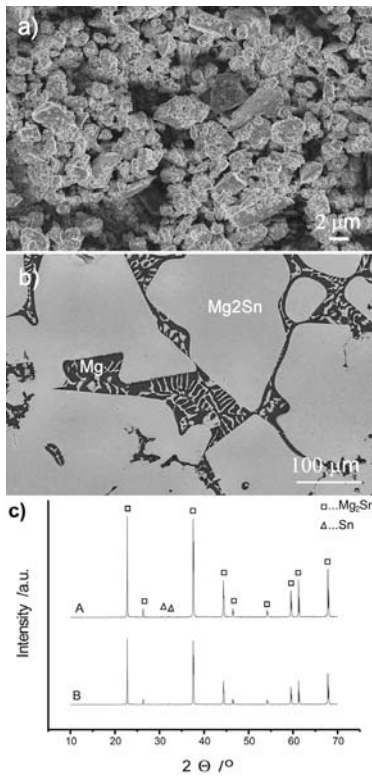
Figure 1: a) SEM micrograph of Mg$_2$Sn powder (grade B) after milling, **b**) SEM micrograph of as-synthesized Mg$_2$Sn and **c**) X-ray powder diffraction pattern of the prepared compound Mg$_2$Sn: A – grade B powder (**Table 1**), and B – grade C powder (**Table 1**)

Slika 1: a) SEM-posnetek Mg$_2$Sn prahu (tip B) po mletju, **b**) SEM-posnetek vzorca Mg$_2$Sn pred mletjem in **c**) XRD-difraktogram sintetizirane Mg$_2$Sn-spojine: A – tip B (**Tabela 1**) in B-tip C (**Tabela 1**)
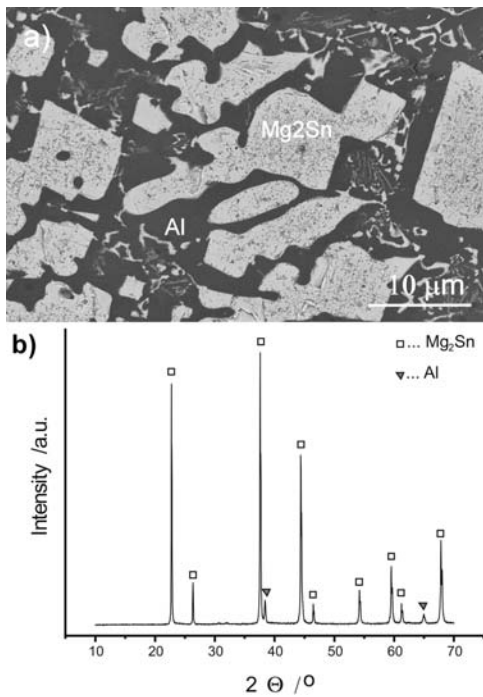

Figure 2: a) SEM micrograph and **b**) X-ray powder-diffraction pattern of the pressurelessly infiltrated Mg$_2$Sn-Al composite sample

Slika 2: a) SEM-posnetek in **b**) XRD-difraktogram Mg$_2$Sn-Al-kompozita, pripravljenega z infiltracijo
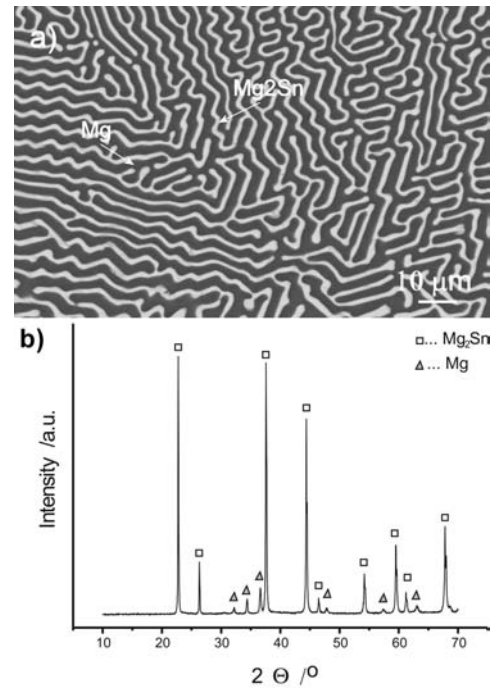

Figure 3: a) SEM micrograph and **b**) X-ray powder diffraction pattern of the Mg$_2$Sn-Mg composite sample infiltrated at 730 °C showing a lamellar structure consisting of Mg$_2$Sn "Chinese-script" in a matrix of magnesium

Slika 3: a) SEM-posnetek in **b**) XRD-difraktogram Mg$_2$Sn-Mg-kompozita, infiltriranega pri 730 °C z značilno lamelarno mikrostrukturo ojačitve v Mg matriki
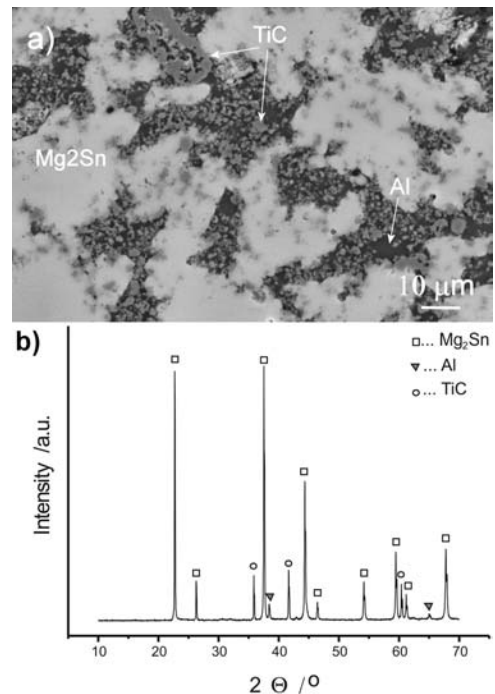

Figure 4: a) SEM micrograph and **b**) XRD spectrum of pressureless infiltrated Al-Sn-Mg$_2$Sn$_{(p)}$-TiC$_{(p)}$ composite sample with an initial composition of the preform skeleton of φ = 69 % Mg$_2$Sn, φ = 29 % TiC and φ = 2 % Al (volume fraction φ/%)

Slika4: a) SEM posnetk in **b**) XRD difraktogram vzorca Al-Sn-Mg$_2$Sn$_{(p)}$-TiC$_{(p)}$ – kompozita, izdelanega z infiltriracijo predoblike na osnovi 69 % Mg$_2$Sn, 29 % TiC in 2 % Al (volumenski delež φ/%)

Table 3: Average room-temperature Vickers hardness and fracture toughness of Al-Mg₂Sn composites prepared by pressureless infiltration
Tabela 3: Povprečne vrednosti trdote po Vickersu in prelomne žilavosti, izmerjene pri sobni temperaturi na vzorcih Al-Mg₂Sn-kompozitov, izdelanih s postopkom infiltracije

Composite composition $\varphi/\%$	Retained porosity $\varphi/\%$	Density $\rho/(g/cm^3)$	Vickers hardness (GPa)	$K_{IC}/$ (MPa m$^{1/2}$)
18 % Al-82 % Mg₂Sn	2.2 ± 0.2	3.5 ± 0.4	0.87 ± 0.09	3.4 ± 0.4
29 % Al-71 % Mg₂Sn	3.5 ± 0.4	3.4 ± 0.3	0.82 ± 0.08	4.7 ± 0.5
38 % Al-62 % Mg₂Sn	4.7 ± 0.5	3.3 ± 0.3	0.75 ± 0.08	5.3 ± 0.5
19 % Al-81 % Mg₂Sn	2.0 ± 0.2	3.6 ± 0.4	0.88 ± 0.09	3.9 ± 0.4
28 % Al-72 % Mg₂Sn	3.2 ± 0.3	3.5 ± 0.4	0.83 ± 0.08	4.8 ± 0.5
38 % Al-62 % Mg₂Sn	3.9 ± 0.4	3.4 ± 0.3	0.79 ± 0.08	5.6 ± 0.6

Table 4: Average room-temperature Vickers hardness and fracture toughness of Mg-Sn-Mg₂Sn composites prepared by pressureless infiltration
Tabela 4: Povprečne vrednosti trdote po Vickersu in prelomne žilavosti, izmerjene pri sobni temperaturi na vzorcih Mg-Sn-Mg₂Sn-kompozita, izdelanega s postopkom infiltracije

Composite composition $\varphi/\%$	Retained porosity $\varphi/\%$	Density $\rho/(g/cm^3)$	Vickers hardness (GPa)	$K_{IC}/$ (MPa m$^{1/2}$)
20 % Mg-80 % Mg₂Sn	2.2 ± 0.2	3.3 ± 0.3	0.66 ± 0.07	4.7 ± 0.5
28 % Mg-71 % Mg₂Sn	3.5 ± 0.4	3.1 ± 0.3	0.72 ± 0.07	6.5 ± 0.7
41 % Mg-59 % Mg₂Sn	4.7 ± 0.5	2.9 ± 0.3	0.77 ± 0.08	7.3 ± 0.7
19 % Mg-81 % Mg₂Sn	2.0 ± 0.2	3.4 ± 0.4	0.61 ± 0.06	5.4 ± 0.5
31 % Mg-69 % Mg₂Sn	3.2 ± 0.3	3.1 ± 0.4	0.69 ± 0.07	6.6 ± 0.7
38 % Mg-62 % Mg₂Sn	3.9 ± 0.4	3.0 ± 0.3	0.71 ± 0.07	7.7 ± 0.8

was proved with the corresponding X-ray diffraction patterns, **Figures 2b** and **3b**.

As evident from **Tables 3** and **4**, the Vickers hardnesses of the Al-Mg₂Sn and Mg-Mg₂Sn MMCs are improved with increasing the amount of Mg₂Sn particulate reinforcement. However, regarding the fracture toughness, quite the opposite behaviour was observed. The fracture toughness of Al-Mg₂Sn and Mg-Mg₂Sn MMCs decreases with an increasing amount of Mg₂Sn particulates.

Comparing the mechanical properties of the Al-Mg₂Sn and Mg-Mg₂Sn MMCs, it is found that the Vickers hardness is evidently better in the samples infiltrated with aluminium. However, the fracture toughness is an exception, becoming greater (almost doubled) in the samples infiltrated with magnesium.

The extraordinary fracture toughness of Mg-Mg₂Sn MMCs is caused by their characteristic lamellar structure consisting of Mg₂Sn "Chinese script" in a matrix of a magnesium solid solution.

3.2.2 Al-Mg₂Sn₍ₚ₎-TiC₍ₚ₎ and Al-Mg₂Sn₍ₚ₎-TiB₂₍ₚ₎

Preforms made from mixtures of laboratory-synthesized Mg₂Sn powder and commercially available TiC and TiB₂ powders (compositions #1, #2, #3 and #4), were also successfully pressurelessly infiltrated with molten aluminium, resulting in samples with almost theoretical density and interesting combinations of mechanical properties.

The microstructure of infiltrated samples consisted of a co-continuous network of Mg₂Sn phase interpenetrated by an aluminium matrix with finely dispersed TiC or TiB₂ particles, **Figures 4** and **5**. The absence of secondary phases, **Figure 5b**, indicates that in this case the spontaneous infiltration also proceeded as a non-reactive process.

The reinforcement of an Al matrix with TiC or TiB₂ particles resulted in a marked improvement in the Vickers hardness. As evident from **Table 5**, the Vickers hardness of Al-Mg₂Sn-TiC and Al-Mg₂Sn-TiB₂ composites was approximately 50 % higher than in non-reinforced Al-Mg₂Sn samples, **Table 3**.

An examination of the fracture toughness, **Table 5**, revealed that the toughness of the MMCs was inversely proportional to the total amount of reinforcing phase. Moreover, it became lower when replacing some of the Mg₂Sn particles with more brittle TiC or TiB₂ particulates. This is well documented in **Tables 3 and 5** for samples with approximately the same total amount of particulate reinforcement.

3.2.3 Mg -Mg₂Sn₍ₚ₎-TiC₍ₚ₎ and Mg-Mg₂Sn₍ₚ₎-TiB₂₍ₚ₎

The experiments showed that the infiltration of Mg₂Sn-TiC and Mg₂Sn-TiB₂ preforms with molten magnesium proceeded spontaneously, without a chemical reaction between the preform skeleton and the molten magnesium. By adjusting the porosity of the preforms within the range the volume fractions of 30 % to 35 %, composites with different compositions listed in Table 6 were routinely fabricated. At 900 °C, the infiltration was complete within 1h, resulting in composite samples with less than φ = 5 % of retained porosity.

The resulting composite samples have a typical eutectic microstructure showing a lamellar structure consisting of Mg₂Sn "Chinese script" in a matrix of
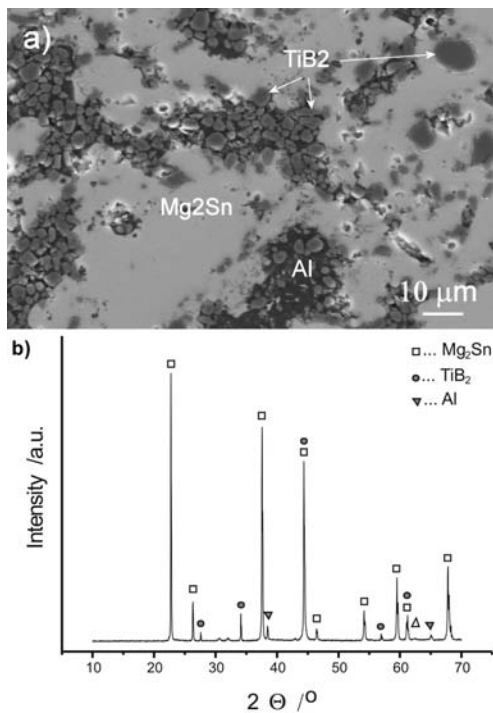
Figure5: a) SEM micrograph and **b**) XRD spectrum of pressurelessly infiltrated Al-Sn-Mg$_2$Sn$_{(p)}$-TiB$_{2(p)}$ composite sample with an initial composition of the preform skeleton φ = 75 % Mg$_2$Sn, φ = 25 % TiB$_2$.
Slika 5: a) SEM-posnetek in **b**) XRD-defraktogram vzorca Al-Sn-Mg$_2$Sn$_{(p)}$-TiB$_{2(p)}$ –kompozita, izdelanega iz predoblike na osnovi φ = 75 % Mg$_2$Sn in φ = 25 % TiB$_2$
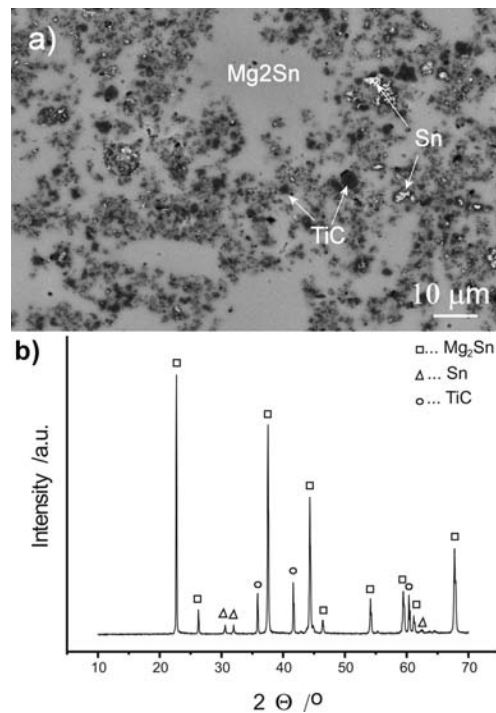

Figure7: a) SEM micrograph and **b**) XRD spectrum of pressurelessly sintered Mg$_2$Sn-Sn-TiC$_{(p)}$ composite sample with the initial composition φ = 67 % Mg$_2$Sn, φ = 3 % Sn and φ = 30 % TiC
Slika7: a) SEM-posnetek in **b**) XRD-difraktogram Mg$_2$Sn-Sn-TiC$_{(p)}$ -kompozita, izdelanega s sintranjem vzorcev, sestavljenih iz φ = 67 % Mg$_2$Sn, φ = 3 % Sn in φ = 30 % TiC
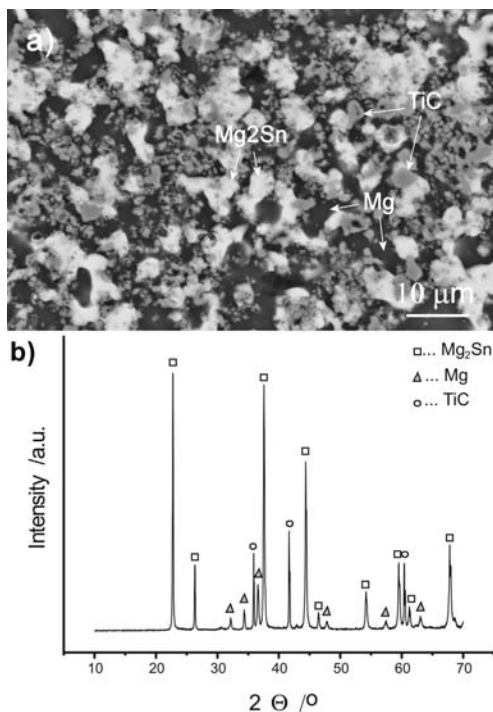

Figure6: a) SEM micrograph and **b**) XRD spectrum of Mg-Sn-Mg$_2$Sn$_{(p)}$-TiC$_{(p)}$ with an initial composition of the preform skeleton φ = 70 % Mg$_2$Sn and φ = 30 % TiC
Slika6: a) SEM-posnetek in **b**) XRD-defraktogram vzorca Mg-Sn-Mg$_2$Sn$_{(p)}$-TiC$_{(p)}$-kompozita, izdelanega z infiltracijo predoblike na osnovi φ = 70 % Mg$_2$Sn in φ = 30 % TiC

magnesium solid solution, additionally reinforced with fine TiC or TiB$_2$ particles, **Figures 7a and 8a**.

From the X-ray diffraction patterns of the composite samples, it is evident (**Figure 7b and 8b**) that besides Mg$_2$Sn reinforcement and irrespective of the matrix composition, no secondary phases were detected, which indicates that the pressureless infiltration of Mg$_2$Sn preforms with molten Mg-Sn-based alloys was not chemically assisted. A detailed SEM examination of interface regions of all the samples also confirmed the absence of chemical reactions between the composite constituents listed above.

Regarding the mechanical properties of the Mg-Mg$_2$Sn-TiC and Mg-Mg$_2$Sn-TiB$_2$ composite samples, which are summarized in **Table 6**, an increase in the particulate content (Mg$_2$Sn and TiC or TiB$_2$) was observed to improve the Vickers hardness, while at the same time reducing the fracture toughness. In addition, the Vickers hardness of the Mg-Mg$_2$Sn-TiC and Mg-Mg$_2$Sn-TiB$_2$ composite samples was found to be better than in the non-reinforced counterparts, while the fracture toughness was about 25 % lower.

Compared to the Al-Mg$_2$Sn-TiC or Al-Mg$_2$Sn-TiB$_2$ counterparts, the reduction of Vickers hardness is only slight. On the other hand, the fracture toughness of the Mg-Mg$_2$Sn-TiC or Mg-Mg$_2$Sn-TiB$_2$ composites is almost twice as high as in their Al-Mg$_2$Sn-TiC or Al-Mg$_2$Sn-TiB$_2$ counterparts, which is due to the lamellar structure

consisting of the Mg$_2$Sn "Chinese script" in a matrix of magnesium.

3.3 Composites made by pressureless sintering

3.3.1 Mg$_2$Sn-Sn-TiC$_{(p)}$ and Mg$_2$Sn-Sn-TiB$_{2(p)}$ composites made by pressureless sintering

Pressureless sintering of green samples made either from as-milled Mg$_2$Sn powders of grade A and B, **Table 1**, or mixed with various amounts of TiC or TiB$_2$ particles, resulted in dense composite specimens with a retained porosity of less than the volume fraction $\varphi = 5$ %. In contrast, pressureless sintering of green samples made either from as-milled Mg$_2$Sn powder of grade C, **Table 1**, or mixed with various amounts of TiC or TiB$_2$ particles, was found to be incomplete, with more than $\varphi = 10$ % of retained porosity.

Table 5: Average room-temperature Vickers hardness and fracture toughness of Al-Sn-Mg$_2$Sn$_{(p)}$(grade C)-TiC$_{(p)}$ and Al-Sn-Mg$_2$Sn$_{(p)}$(grade A)-TiB$_{2(p)}$ composites prepared by pressureless infiltration

Tabela 5: Povprečne vrednosti trdote po Vickersu in prelomne žilavosti, izmerjene pri sobni temperaturi na vzorcih Al-Sn-Mg$_2$Sn$_{(p)}$(tip C)-TiC$_{(p)}$ and Al-Sn-Mg$_2$Sn$_{(p)}$(tip A)-TiB$_{2(p)}$- kompozitov, izdelanih s postopkom infiltracije

Composite composition φ/%	Retained porosity φ/%	Density ρ/(g/cm^3)	Vickers hardness (GPa)	K_{IC}/ (MPa m$^{1/2}$)
28%Al-48%Mg$_2$Sn-23 %TiC	1.9 ± 0.2	3.6 ± 0.2	1.29 ± 0.13	2.8 ± 0.3
36%Al-46%Mg$_2$Sn-18 %TiC	2.2 ± 0.2	3.5 ± 0.2	1.14 ± 0.11	3.1 ± 0.3
28%Al-49%Mg$_2$Sn-23%TiB$_2$	3.5 ± 0.4	3.6 ± 0.2	1.38 ± 0.14	2.7 ± 0.3
35%Al-46%Mg$_2$Sn-19%TiB$_2$	4.7 ± 0.5	3.5 ± 0.2	1.26 ± 0.13	3.0 ± 0.3

Table 6: Average room-temperature Vickers hardness and fracture toughness of Mg- Mg$_2$Sn$_{(p)}$-TiC$_{(p)}$ and Mg-Mg$_2$Sn$_{(p)}$-TiB$_{2(p)}$ composites prepared by pressureless infiltration

Tabela 6: Povprečne vrednosti trdote po Vickersu in prelomne žilavosti, izmerjene pri sobni temperaturi na vzorcih Al-Sn-Mg$_2$Sn$_{(p)}$(tip C)-TiC$_{(p)}$ in Al-Sn-Mg$_2$Sn$_{(p)}$(tip A)-TiB$_{2(p)}$-kompozitov, izdelanih s postopkom infiltracije

Composite composition φ/%	Retained porosity φ/%	Density ρ/(g/cm^3)	Vickers hardness (GPa)	K_{IC}/ (MPa m$^{1/2}$)
29% Mg-47%Mg$_2$Sn-1%Al-23 %TiC	1.9±0.2	3.4±0.2	1.16±0.12	4.9±0.5
36%Mg-38%Mg$_2$Sn-7%Al–19%TiC	2.2±0.2	3.5±0.2	1.0±0.19	5.8±0.6
29%Mg-48%Mg$_2$Sn–1%Al-22%TiB$_2$	3.5±0.4	3.3±0.2	1.24±0.12	4.4±0.4
35%Mg-39%Mg$_2$Sn–7%Al-19%TiB$_2$	4.7±0.5	3.3±0.2	1.13±0.11	5.3±0.5

Table 7: Average room-temperature Vickers hardness and fracture toughness of sintered Mg$_2$Sn -Sn-TiC samples.

Tabela 7: Povprečne vrednosti trdote po Vickersu in prelomne žilavosti, izmerjene pri sobni temperaturi na vzorcih, sintranih Mg$_2$Sn -Sn-TiC-kompozitov

Composite initial composition φ/%	Retained porosity φ/%	Density ρ/(g/cm^3)	Vickers hardness (GPa)	K_{IC}/ (MPa m$^{1/2}$)
97% Mg$_2$Sn (grade A)-3% Sn	4.8 ± 0.5	3.7 ± 0.2	1.0 ± 0.1	1.7 ± 0.2
87% Mg$_2$Sn (grade A)-3% Sn-10% TiC	3.5 ± 0.4	3.8 ± 0.2	1.4 ± 0.1	1.4 ± 0.1
68% Mg$_2$Sn (grade A)-2% Sn-30% TiC	4.3 ± 0.4	4.1 ± 0.4	1.5 ± 0.2	1.0 ± 0.1
49% Mg$_2$Sn (grade A)-1% Sn-50% TiC	4.9 ± 0.5	4.3 ± 0.5	1.8 ± 0.2	0.7 ± 0.1
95% Mg$_2$Sn (grade B)-5% Sn	3.1 ± 0.3	3.8 ± 0.5	0.9 ± 0.1	1.8 ± 0.2
86% Mg$_2$Sn (grade B)-4% Sn-10% TiC	2.7 ± 0.3	3.8 ± 0.3	1.0 ± 0.1	1.4 ± 0.1
66% Mg$_2$Sn (grade B)-3% Sn-30% TiC	3.9 ± 0.4	3.9 ± 0.4	1.3 ± 0.1	1.1 ± 0.1
48% Mg$_2$Sn (grade B)-2% Sn-50% TiC	4.1 ± 0.5	4.1 ± 0.5	1.7 ± 0.2	0.6 ± 0.1

Table 8: Average room-temperature Vickers hardness and fracture toughness of sintered Mg$_2$Sn-Sn-TiB$_2$ composite samples

Tabela 8: Povprečne vrednosti trdote po Vickersu in prelomne žilavosti, izmerjene pri sobni temperatri na vzorcih, sintranih Mg$_2$Sn-Sn-TiB$_2$-kompozitov

Composite initial composition) φ/%	Retained porosity φ/%	Density ρ/(g/cm^3)	Vickers hardness (GPa)	K_{IC}/ (MPa m$^{1/2}$)
97 % Mg$_2$Sn (grade A)-3 % Sn	4.8 ± 0.5	3.7 ± 0.2	1.0 ± 0.1	1.7 ± 0.2
87 % Mg$_2$Sn (grade A)-3 % Sn-10 % TiB$_2$	3.5 ± 0.4	3.8 ± 0.2	1.5 ± 0.1	1.3 ± 0.1
68 % Mg$_2$Sn (grade A)-2 % Sn-30 % TiB$_2$	4.3 ± 0.4	4.1 ± 0.4	1.7 ± 0.2	0.8 ± 0.1
49 % Mg$_2$Sn (grade A)-1 % Sn-50 % TiB$_2$	4.9 ± 0.5	4.3 ± 0.5	1.9 ± 0.2	0.6 ± 0.1
95 % Mg$_2$Sn (grade B)-5 % Sn	3.1 ± 0.3	3.8 ± 0.5	0.9 ± 0.1	1.8 ± 0.2
86 % Mg$_2$Sn (grade B)-4 % Sn-10 % TiB$_2$	2.7 ± 0.3	3.8 ± 0.3	1.0 ± 0.1	1.4 ± 0.1
66 % Mg$_2$Sn (grade B)-3 % Sn-30 % TiB$_2$	3.9 ± 0.4	3.9 ± 0.4	1.6 ± 0.1	1.0 ± 0.1
48 % Mg$_2$Sn (grade B)-2 % Sn-50 % TiB$_2$	4.1 ± 0.5	4.1 ± 0.5	2.0 ± 0.2	0.5 ± 0.1

The microstructure of the sintered samples reinforced with ceramic particulates is presented in **Figures 7 and 8**. The composites obtained consist of a continuous Mg_2Sn matrix and TiC or TiB_2 ceramic particulate reinforcement dispersed around the sintered Mg_2Sn grains and small Sn inclusions. In contrast, the microstructure of the dense, non-reinforced samples was uniform, with fully sintered Mg_2Sn grains and Sn inclusions.

The SEM-EDS evaluation of the samples and the XRD measurements imply that the Mg_2Sn-TiC and Mg_2Sn-TiB_2 systems are non-reactive, without secondary phases formed during the sintering, and that the sintering proceeded via a non-reactive mechanism, assisted by the liquid Sn phase. The mechanical properties of the sintered samples are listed in **Tables 7 and 8**.

The Vickers hardness of the pressurelessly sintered samples was found to be enhanced with an increasing amount of particulate reinforcement in the Mg_2Sn matrix, **Table 2**. In addition, the Vickers hardness measurements also confirmed that the sintering of samples with the same initial volume fraction of TiC or TiB_2 reinforcement resulted in composites with similar hardnesses. This is most probably caused by the similar microstructures of the Mg_2Sn-TiC and Mg_2Sn-TiB_2-composite samples, the same sintering mechanism and almost the same hardness of the TiC and TiB_2 reinforcing particulates.

4 CONCLUSIONS

The reactive synthesis of Mg_2Sn from the elements resulted in a high-yield, single-phase product with less than the mass fraction 0.2 % of impurities (Mg or Sn), depending on the composition of the initial reactive mixture.

1. Additional crushing and subsequent milling of the reaction product (i.e., in a planetary mill) was found to be an easy operation, enabling the cost-effective preparation of Mg_2Sn powders with an average particle size of less than 5 μm, suitable for the production of Mg_2Sn-based advanced composites.

2. Depending on the selected synthesis technique of (i) **pressureless infiltration** of porous Mg_2Sn, Mg_2Sn-TiC and Mg_2Sn-TiB_2 preforms with molten aluminium and magnesium, or (ii) **pressureless sintering** of green Mg_2Sn-TiC and Mg_2Sn-TiB_2 compacts, Mg_2Sn-based composites of different nature, microstructure and combination of properties were successfully prepared, demonstrating the significant potential of the Mg_2Sn phase as a composite matrix and of the particulate reinforcement.

3. The investigation of the effect of different microstructures developed in Mg_2Sn-based composites on their mechanical properties (hardness and toughness) revealed that Mg_2Sn, as the stoichiometric compound, could be useful for tailoring an optimum combination of these properties.

4. The pressureless infiltration of porous Mg_2Sn, Mg_2Sn-TiC and Mg_2Sn-TiB_2 preforms with molten magnesium and aluminium resulted in dense ($\geq$95 % T.D.) metal matrix composites with a metallic matrix discontinuously reinforced with Mg_2Sn and TiC or TiB_2 particulates. The infiltration proceeded spontaneously, without detectable chemical reactions between the preform skeleton and the molten infiltrants.

5. The composite samples infiltrated with molten magnesium possessed the characteristic lamellar "Chinese script" eutectic microstructure, while in samples infiltrated with molten aluminium the appearance of fine Mg_2Sn-Sn precipitates in an Al matrix, mostly in the vicinity of the initially introduced Mg_2Sn particles, was observed.

6. In preforms with the addition of TiC or TiB_2 ceramic reinforcement, the microstructure development during the infiltration occurred in the same way as in their non-reinforced counterparts. Because of the low temperature of the preform infiltration (750 °C), the particulate reinforcements remained chemically inert in contact with molten magnesium or molten aluminium, resulting in a final microstructure of infiltrated composite samples the same as in the non-reinforced counterparts. The only difference was observed inside the Al or Mg phases, which were completely reinforced with TiC or TiB_2 particles.

7. The microstructure of the composite samples obtained by pressureless infiltration could be tailored to consist of a continuous aluminium or magnesium matrix, discontinuously reinforced with Mg_2Sn of different morphologies (particulates in samples infiltrated with aluminium and the characteristic "Chinese script" eutectic phase in samples infiltrated with magnesium) and, when added, TiC or TiB_2 reinforcements. Such a microstructure design was projected in order to achieve an optimum combination of enhanced fracture toughness (particularly improved by the "Chinese script" phase appearing in samples infiltrated with magnesium), with tensile properties and a hardness superior to that of conventional Mg-Sn alloys.

8. The Vickers hardness was found to be better in samples infiltrated with aluminium than in counterparts infiltrated with magnesium. On the other hand, quite the opposite behaviour was found with regard to the fracture toughness. Due to their characteristic lamellar structure consisting of Mg_2Sn as the "Chinese script" in the matrix, composite samples infiltrated with magnesium possessed an enhanced fracture toughness almost twice that of the counterparts infiltrated with aluminium, in which the Mg_2Sn phase appeared as particulates.

9. Within each single group of infiltrated samples (i.e., samples with the same *qualitative* composition), the Vickers hardness was enhanced, while the fracture

toughness decreased with an increasing total amount of particulate reinforcement.

10. Pressureless sintering of green samples from Mg_2Sn powders with 3–5% of free Sn, or from mixtures of these powders with various amounts of TiC or TiB_2 particles, resulted in dense composite specimens with a porosity of less than the volume fraction $\varphi = 5$ %. In contrast, pressureless sintering of green samples from Mg_2Sn powder without free Sn or a mixture of the same powder with various amounts of TiC or TiB_2 particles was found to be incomplete, with more than $\varphi = 10$ % of porosity.

11. The composites obtained consisted of a continuous Mg_2Sn matrix and TiC or TiB_2 ceramic particulate reinforcement dispersed around the sintered Mg_2Sn grains and small Sn inclusions. In contrast, the microstructures of the dense, non-reinforced samples were uniform, with fully sintered Mg_2Sn grains and Sn inclusions.

12. During sintering, the formation of secondary phases was not observed. Densification of composite samples proceeded with non-reactive sintering, assisted by molten tin

13. The Vickers hardness of the sintered samples (intermetallic matrix composites with a Mg_2Sn matrix discontinuously reinforced with TiC or TiB_2 ceramic reinforcement) was significantly improved in comparison with the metal matrix composites obtained by infiltration. The exception was the fracture toughness, which in the sintered samples was reduced to approximately one-third or even one-quarter of the values measured in the metal matrix composites obtained by infiltration.

14. With densities higher than the density of aluminium and magnesium alloys, Mg_2Sn-based composites have a limited potential for the weight reduction of structural parts. However, some of the Mg_2Sn composites (especially Mg-Mg_2Sn metal matrix composites) could offer a unique combination of properties, including the ability of the composite microstructure (lamellar, consisting of the Mg_2Sn "Scinese script" in a magnesium solid solution) to develop a toughening mechanism in combination with improved tensile properties and hardness.

Acknowledgement

5 REFERENCES

[1] N. Hort, Y. Huang, T. A. Leil, P. Maier, K. U. Kainer, Adv. Eng. Mat., 8 (**2006**) 5, 359

[2] N. Hort, Y. Huang, K. U. Kainer, F. Moll, K. U. Kainer, Adv. Eng. Mat., 8 (**2006**) 4, 235

[34] J. Gröbner, A. Janz, A. Kozlov, Dj. Mirković, R. S. Fetzer, JOM, 60 (**2009**) 12, 32

[4] M. Zhang, W. Z. Zhang, G. Z. Zhu, Scrpita Materialia 59 (**2008**), 866

[5] Z. Min, Z. W. Zheng, Z. G. Zhen, Y. Kun, Trans. Nonferrous Met. China 17 (**2007**), 1428

[6] Z. X. Ping, C. Y. Gui, X. Y. HUa, Trans Nonferrous Met. Soc. China 18 (**2008**), s299

[7] B. H. Kim, J. J. Jeon, K. C. Park, B. G. Park, Y. H. Park, I. M. park, Archives of Materials Science and Engineering, 30 (**2008**) 2, 93

[8] S. Koch, H. Antrekowitsch, BHM, 153 (**2008**) 7, 278

[9] O. Madelung, U. Rössler, M. Schulz, Non-tetrahedrally bonded elements and binary compounds I, Springer-Verlag, 1998, 1–3

[10] C. Zhang, P. Han, X. Yan, C. Wang, L. Xia, B. Xu, J. Phys. D: Appl. Phys., 42 (**2009**), 1. (doi: 125403)

[11] W. Y. Feng, D. W. Bo, Z. T. Young, Trans. Nonferrous Met. Soc. China, 19 (**2009**), 1196

[12] K. Kondoh, H. Oginuma, T. Aizawa, Materials Transactions, 42 (**2001**), 1293

[13] K. Niihara, R. Morena, D. P. Hasselman, J. Mater. Sci. Lett. 1 (**1982**), 13

[14] A. A. Nayeb-Hasemi, J. B. Clark, J. Bull. Alloy Phase Diagrams 63 (**1984**), 467